DIGITAL ACCESS TO SCHOLARSHIP AT HARVARD
DASH.HARVARD.EDU

HARVARD LIBRARY
Office for Scholarly Communication

Asymmetry in the Clockwise and Counter-Clockwise Rotation of the Bacterial Flagellar Motor

Citation
Yuan, Junhua, Karen A. Fahrner, Linda Turner, and Howard C. Berg. 2010. Asymmetry in the clockwise and counter-clockwise rotation of the bacterial flagellar motor. Proceedings of the National Academy of Science 107(29): 12846-12849.

Published Version
doi:10.1073/pnas.1007333107

Permanent link
http://nrs.harvard.edu/urn-3:HUL.InstRepos:4322129

Terms of Use
This article was downloaded from Harvard University's DASH repository, and is made available under the terms and conditions applicable to Other Posted Material, as set forth at http://nrs.harvard.edu/urn-3:HUL.InstRepos:dash.current.terms-of-use#LAA

Share Your Story

The Harvard community has made this article openly available.
Please share how this access benefits you. Submit a story .

Accessibility

BIOLOGICAL SCIENCES: Biophysics

Asymmetry in the clockwise and counter-clockwise rotation of the bacterial flagellar motor

Junhua Yuan, Karen A. Fahrner, Linda Turner & Howard C. Berg

Department of Molecular and Cellular Biology, Harvard University, Cambridge, MA 02138, and Rowland Institute for at Harvard, Cambridge, MA 02142

Corresponding author: Howard C. Berg, Department of Molecular and Cellular Biology, Harvard University, Biological Laboratories, 16 Divinity Avenue, Cambridge, MA 02138, tel 617-495-0924, fax 617-496-1114, e-mail *hberg@mcb.harvard.edu*

Cells of *Escherichia coli* are able to swim up gradients of chemical attractants by modulating the direction of rotation of their flagellar motors, which spin alternately clockwise (CW) and counter-clockwise (CCW). Rotation in either direction has been thought to be symmetric and exhibit the same torques and speeds. The relationship between torque and speed is one of the most important measurable characteristics of the motor, used to distinguish specific mechanisms of motor rotation. Previous measurements of the torque-speed relationship have been made with cells lacking the response regulator CheY that spin their motors exclusively CCW. In this case, the torque declines slightly up to an intermediate speed called the "knee speed" after which it falls rapidly to zero. This result is consistent with a "power-stroke" mechanism for torque generation. Here, we measure the torque-speed relationship for cells that express large amounts of CheY and only spin their motors CW. We find that the torque decreases linearly with speed, a result remarkably different from that for CCW rotation. We obtain similar results for wild-type cells by re-examining data collected in previous work. We speculate that CCW rotation might be optimized for runs, with higher speeds increasing the ability of cells to sense spatial gradients, while CW rotation might be optimized for tumbles, where the object is to change cell trajectories. But why a linear torque-speed relationship might be optimum for the latter purpose we do not know.

nano-gold motility molecular motor switch torque-speed

Measurements of the torque-speed relationship of the bacterial flagellar motor provide a crucial test of models for motor rotation (1-2). Previous measurements of this relationship have been made with smooth-swimming (CCW-rotating) mutants of a variety of species: with the proton-driven motor of *Escherichia coli* (3-4), with the sodium-driven motor of *Vibrio alginolyticus* (5), and with a sodium-driven chimeric motor in *E. coli* (6). In all cases, motor torque is approximately constant up to a knee speed, after which it drops rapidly to zero. In *E. coli* at room temperature, the knee speed is about 170 Hz, and the zero-torque speed is about 300 Hz. It has been assumed that CCW and CW rotation are symmetric and exhibit the same torques and speeds (7).

Here, we measured the torque-speed relationship for an *E. coli* strain locked in CW rotation. This strain is deleted for the genes that encode the response regulator, CheY, and its phosphatase, CheZ, as well as the adaptation enzymes CheR and CheB. Introduction of a plasmid that encodes wild-type CheY that can be induced to high levels with isopropyl β-D-thiogalactoside (IPTG) enables CW rotation. For comparison, we also measured the torque-speed relationship with the same strain lacking the plasmid, which is locked in CCW rotation. The measurements were made by adsorbing 0.356-μm-diameter latex spheres to sticky-filament stubs (8) and monitoring rotation rates in motility medium containing different concentrations of the viscous agent Ficoll (0-15%) and by attaching 60-nm-diameter gold spheres to hooks of strains that lack flagellar filaments (9) and monitoring rotation rates in motility medium. Also, we reexamined data obtained earlier from wild-type cells with filament stubs labeled with latex spheres

of various sizes or with full-length filaments labeled with fluorescent dye that did not undergo polymorphic transformations upon flagellar reversal.

Results

Figure 1 shows the torque-speed relationships for CCW (red triangles and lines) and CW rotation (green squares and line) for the mutant strains designed for this study. The symbols are means and standard deviations, while the lines are linear regressions. The measurements were made with 0.356-μm-diameter latex beads on sticky filament stubs in motility medium containing different amounts of Ficoll and with 60-nm-diameter gold spheres on hooks in motility medium, as specified in the figure legend. All torques were normalized to the CCW torque determined for 0.356-μm-diameter beads on filament stubs in 15% Ficoll, a normalization that preserves the relative shapes of the CW and CCW curves. The line for CW rotation is a simple linear regression, while the lines for CCW rotation are two linear regressions, the first for the first four data points and the second for the fourth to ninth data points. The point of intersection of the two lines indicates the knee speed. For CCW rotation, motor torque fell ~10% between 0 and ~190 Hz and then dropped rapidly, reaching 0 at ~285 Hz, in agreement with previous measurements made at room temperature (3-4). For CW rotation, on the other hand, motor torque decreased linearly with speed, reaching 0 at ~265 Hz. The stall torques (the torques at zero speed) for both directions were approximately the same, as were the zero-torque speeds.

The relative positions of the CW and CCW curves in Fig. 1 could be different if shifts in the shape of the hook and filament due to differences in direction changed the distance between the rotation axis and the center of the bead, and hence the load. We think this is not a serious problem, because the flagella were well-sheared and differences of bead-path trajectories observed with wild-type cells (discussed in the second paragraph below) were relatively small. With wild-type cells, one can look at the same bead on the same cell spinning in either direction. With CW and CCW mutants, this is not possible, because one is comparing different beads on different cells, with the shape of the measured bead trajectory depending upon the positions of the detectors and the detector gains. With 60-nm-diameter gold spheres on hooks, the load remains close to zero for all trajectories, so changes in trajectories do not matter.

Earlier, we measured the performance of wild-type motors switching at various loads, using beads with different diameters and motility medium containing different concentrations of Ficoll (10-11). We plotted the CCW and CW speeds determined earlier against each other (Fig. 2A, filled circles with error bars). From the torque-speed curves of Fig. 1, similar results can be obtained by the method illustrated in Fig. 2B, assuming that the load did not change with direction. These are shown by the magenta curve in Fig. 2A. The two sets of measurements agree. Note that the strains used in previous measurements were derived from AW405 (12), while the strains used in this study were derived from RP437 (13), a descendent of AW405. The CCW zero-torque speed of the strains derived from AW405 was about 350Hz, while the CCW zero-torque speed for the strains derived from RP437 was about 285 Hz, a difference that might be due to

differences in the protonmotive force (pmf). Therefore, the comparisons of Fig. 2A were made by scaling both torque and speed for the torque-speed curves of Fig. 1 by a factor of 350/285, according to the linear dependence of torque-speed curves on pmf established previously (14).

To correct for possible effects of variation in load when wild-type motors switch, we compared the bead trajectories for CW and CCW rotation for all the motors in the data-set shown by filled circles in Fig. 2A. For the motors labeled with gold nano-beads of different size on hooks (the 7 filled circles on the right of Fig. 2A), the trajectory did not change when the motors switched. For the motors labeled with latex beads of different size on filament stubs (the 6 filled circles on the left of Fig. 2A), the major radii of the trajectories for CW and CCW rotation were extracted, as described in Materials and Methods. Load corrections were significant only for the smallest latex bead; the corrected data point is shown in Fig. 2A as the green open square.

CCW and CW speeds also were measured with full-length fluorescent filaments in their normal polymorphic form when motors switched without changing that form (15); the alignment of these filaments remained fixed relative to the cell bodies during these reversals. The CCW and CW speeds are shown as red open circles in Fig. 2**A** and are consistent with the bead data.

Discussion

Measurements of the CCW torque-speed relationship have suggested a power-stroke mechanism, in which a single step couples proton free energy to rotation (16). Subsequent biochemical studies supported this mechanism (2). In *E. coli*, a motor stator complex (anchored to the peptidoglycan layer) is composed of four copies of MotA and two copies of MotB, comprising two proton-conducting transmembrane channels (2). Protonation and subsequent de-protonation of MotB Asp-32 at the cytoplasmic end of either channel is thought to drive conformational changes that exert forces on the periphery of the rotor, via electrostatic interactions between MotA and the rotor protein FliG (17-18). Recently, dynamic models of the flagellar motor incorporating the power stroke mechanism have been proposed (19-22), which explain most features of the CCW torque-speed curve, including its concave shape.

The CW torque-speed curve measured in this work is linear, which also is consistent with a "thermal ratchet" mechanism, in which proton free energy is used to bias movements that are driven thermally (16, 23). But given the biochemical details of the stator complex noted above, this mechanism seems unlikely. However, the linear dependence also can be explained by a power-stroke mechanism. Consider the model proposed by Meacci & Tu, in which the stepping rate of a stator (induced by protons hopping on and off MotB Asp32) depends on the torque exerted by the stator on the rotor (20). Specifically, torque between a stator element and FliG that acts in a direction opposite to that of motor rotation increases the stepping rate of the stator. In this model, the CCW torque-speed curve can be reproduced with a stepping rate during negative torque (k^-) twice the stepping rate during positive torque (k^+). A minor modification of the model, in

which k^+ is close to zero or much smaller than k^-, leads to a torque-speed relationship that is approximately linear (Figure S6 (a) of ref. (20)). CW/CCW switching occurs by movement of the C-terminal domain of FliG at its interface with MotA (24). It might be that differences in the conformations of FliG are responsible for differences in the values of k^+. There is another possibility: in the model proposed by Meacci & Tu, the stator-rotor interaction potential is V-shaped, meaning that the magnitude of the force is constant with respect to the relative position of the stator and rotor. Modification of this potential to a parabolic shape leads to a torque-speed relationship that is nearly linear, with a slight convex shape (Y. Tu, personal communication).

The two torque-speed curves of Fig. 1 match at low and at high speeds but differ in the intermediate-speed range. At low speeds (near stall), the motors operate near thermodynamic equilibrium with nearly 100% efficiency, so the torques are determined by the protonmotive force and are the same for both CW and CCW rotation. At high speed (near zero load), the speed is limited by rates of proton movement and conformational change, which are probably the same whether the rotation is CW or CCW. At intermediate speeds, these rates appear to be affected asymmetrically by the load, and the two torque-speed curves are different.

Cells of *E. coli* are propelled by several helical flagellar filaments, each driven at its base by a reversible rotary motor. When all the motors rotate CCW, the filaments form a bundle that drives the cell steadily forward (in a run). When one or more motors switch to CW, their filaments come out of the bundle and the bacterium moves in an erratic

fashion (in a tumble), resulting in a new direction for the next run (25). It is plausible that mechanisms for CCW rotation have been optimized to achieve maximal swimming speeds, and hence enhanced sensitivity to spatial gradients of chemical attractants, a requirement relevant for runs but not for tumbles. In a tumble, the choice of a new direction is initiated by a motor reversal (from CCW to CW) that causes the filament to unbundle and transform from the left-handed normal form to the right-handed semi-coiled form (15, 25). High rotation speeds might not be required for this maneuver.

While we do not fully understand the functional significance of differences between the CW and CCW torque-speed relationships, these differences provide additional constraints for viable motor models.

Materials and Methods

Strains and plasmids. Strains used for measuring torque-speed relationships were derived from VS149 [Δ(*cheR-cheZ*)] (26), a product of the strain RP437 commonly used in studies of chemotaxis (13). An in-frame deletion of *fliC* was generated to yield JY32. Wild-type *cheY* was cloned into pTrc99A (Amp^R, Pharmacia) under an IPTG-inducible promoter, yielding pWB5. The sticky *fliC* allele was cloned into pACYC184 (Cam^R) under the native promoter of *fliC* (27), yielding pKAF131, a plasmid compatible with pTrc99A. For measurements of the CCW torque-speed relationship, JY32 and JY32 carrying pKAF131 were used. For measurements of the CW torque-speed relationship, JY32 carrying pWB5, and JY32 carrying pWB5 and pKAF131 were used. Cells and Ficoll solutions were prepared as described previously (11).

Experimental procedure. 0.356-μm-diameter latex spheres (Polysciences) were attached to truncated sticky filaments as described previously (28). A tunnel slide was made from a coverslip coated with poly-L-lysine (P4707, Sigma) supported by strips of double sticky tape. A suspension of washed cells was added to the tunnel and incubated for 1 min. Then excess cells were washed away with motility medium. Rotation of the latex spheres was monitored with the laser dark-field setup described previously (11, 29). The measurement of each motor at each Ficoll concentration took 30 s. Exchange of media with different Ficoll concentrations (0, 2, 3, 5, 7, 9, 12 and 15%) was done using 300 μl of media. The volume required (typically 200 μl) to completely displace the previous solution was determined by monitoring motor speeds before, during, and after fluid exchange. The zero-torque measurements with gold spheres were carried out as described previously (9). All experiments were performed at 23°C.

Torque-speed curves. Data analysis was done using custom scripts in MATLAB (MathWorks). Rotational speed was extracted as the peak of the power spectrum for each 30-s data set. Relative torque was computed as speed times rotational frictional drag coefficient (or for beads of the same size, speed times viscosity). For each load, means and standard deviations were computed for the cell ensemble, with each measurement weighted equally. The torques were normalized by dividing by the value for CCW torque with 0.356-μm-diameter beads on filament stubs in 15% Ficoll. The values of viscosity for various concentrations of Ficoll were obtained from measurements made with a Cannon-Ubbelohde capillary viscometer (4).

Speeds for wild-type motors. Speed was determined for each motor as described in the data analysis section of (11), and a histogram was constructed showing the distributions of speeds for each 3 to 5-min measurement. Peak positions at positive and negative velocities were extracted as the CW and CCW speeds. Alternatively, CW and CCW intervals were determined with the threshold-crossing algorithm described in (11), and the peaks of the power spectra of the detector outputs were determined for these intervals. Both methods gave similar results.

If one were to look in a direction parallel to the motor rotation axis, the bead trajectory would be circular. When viewed off-axis, which is the case for most of our observations, this trajectory is elliptical. We took changes in the major radius of this ellipse as a measure of differences in load. The x and y signals were high-pass filtered with a cutoff frequency of 0.5 Hz, and the radius $r = (x^2+y^2)^{1/2}$ was calculated. The maximum r for each revolution was extracted and these numbers were grouped into CW and CCW histograms. The peaks of these histograms were taken as the major radii for the trajectories for CW and CCW rotation.

The ratios of these major radii (CW/CCW) for the 12 motors with 0.356-μm-diameter latex beads were 1.17, 1.00, 1.19, 1.15, 1.16, 0.98, 0.93, 1.19, 1.32, 1.35, 1.19, and 1.04, leading to a mean and standard deviation of 1.14 ± 0.13. The rotational drag coefficients are $f = f_b + f_f$, where f_b and f_f are the drag coefficients of the beads and the filament stubs respectively. $f_b = 8\pi\eta a^3 + 6\pi\eta a l^2$, where η is the viscosity of the medium and a and l are

the radius of the bead and the distance between the rotation axis and the center of the bead (the major radius of the trajectory), respectively. l is about 0.15 um (28), leading to a correction factor for f_b (for the ratio of drag coefficients derived from CW and CCW orbits) of about 1.10. For a 0.356-μm-diameter bead, f_f is about 1/2 f_b (6). So, in the absence of any evidence to the contrary, we assume that the correction factor (CW/CCW) for f also is about 1.10. To convert the correction factor for the drag coefficient into a correction factor for the CW speed, knowledge of the torque-speed curve is required. There are two extreme cases: in the first case, if the torque is constant with speed, the correction factor for speed (CW/CCW) is maximal, and it is the same as that for f: 1.10; in the second case, if the torque drops sharply with speed, the correction factor for speed is 1 (i.e., no correction). In reality, the correction factor for speed is between 1 and 1.10. The two extreme cases are plotted in Fig. 2A, with the filled circle as the uncorrected case and the green square as the corrected case. For larger latex beads, the means of the ratios of major radii (CW/CCW) were closer to 1 (range 0.97-1.02), so their speeds were not corrected.

Acknowledgements

We thank G. Lan and Y. Tu for helpful discussions. This work was supported by National Institutes of Health Grant AI016478.

References

1. Berg HC (2003) The rotary motor of bacterial flagella. *Annu. Rev. Biochem.* 72:19-54.
2. Blair DF (2003) Flagellar movement driven by proton translocation. *FEBS Lett.* 545:86-95.
3. Berg HC & Turner L (1993) Torque generated by the flagellar motor of *Escherichia coli*. *Biophys. J.* 65:2201-2216.
4. Chen X & Berg HC (2000) Torque-speed relationship of the flagellar rotary motor of *Escherichia coli*. *Biophys. J.* 78:1036-1041.
5. Sowa Y, Hotta H, Homma M, & Ishijima A (2003) Torque-speed relationship of the Na^+-driven flagellar motor of *Vibrio alginolyticus*. *J. Mol. Biol.* 327:1043-1051.
6. Inoue Y*, et al.* (2008) Torque-speed relationships of Na^+-driven chimeric flagellar motors in *Escherichia coli*. *J. Mol. Biol.* 376(1251-1259):1251.
7. Blair DF & Berg HC (1988) Restoration of torque in defective flagellar motors. *Science* 242:1678-1681.
8. Scharf BE, Fahrner KA, Turner L, & Berg HC (1998) Control of direction of flagellar rotation in bacterial chemotaxis. *Proc. Natl. Acad. Sci. USA* 95:201-206.
9. Yuan J & Berg HC (2008) Resurrection of the flagellar motor near zero load. *Proc. Natl. Acad. Sci. USA* 105:1182-1185.
10. Fahrner KA, Ryu WS, & Berg HC (2003) Bacterial flagellar switching under load. *Nature* 423:938.

11. Yuan J, Fahrner KA, & Berg HC (2009) Switching of the bacterial flagellar motor near zero load. *J. Mol. Biol.* 390:394-400.

12. Armstrong JB, Adler J, & Dahl MM (1967) Nonchemotactic mutants of *Escherichia coli*. *J. Bacteriol.* 93:390-398.

13. Parkinson JS (1978) Complementation analysis and deletion mapping of *Escherichia coli* mutants defective in chemotaxis. *J. Bacteriol.* 135:45-53.

14. Gabel CV & Berg HC (2003) The speed of the flagellar rotary motor of *Escherichia coli* varies linearly with protonmotive force. *Proc. Natl. Acad. Sci. USA* 100:8748-8751.

15. Darnton NC, Turner L, Rojevsky S, & Berg HC (2007) On torque and tumbling in swimming *Escherichia coli*. *J. Bacteriol.* 189:1756-1764.

16. Berry RM & Berg HC (1999) Torque generated by the flagellar motor of *Escherichia coli* while driven backward. *Biophys. J.* 76:580-587.

17. Zhou J, Lloyd SA, & Blair DF (1998) Electrostatic interactions between rotor and stator in the bacterial flagellar motor. *Proc. Natl. Acad. Sci. USA* 95:6436-6441.

18. Kojima S & Blair DF (2001) Conformational change in the stator of the bacterial flagellar motor. *Biochemistry* 40:13041-13050.

19. Xing J, Bai F, Berry RM, & Oster G (2006) Torque-speed relationship of the bacterial flagellar motor. *Proc. Natl. Acad. Sci. USA* 103:1260-1265.

20. Meacci G & Tu Y (2009) Dynamics of the bacterial flagellar motor with multiple stators. *Proc. Natl. Acad. Sci. USA* 106:3746-3751.

21. Mora T, Yu H, & Wingreen NS (2009) Modeling torque versus speed, shot noise, and rotational diffusion of the bacterial flagellar motor. *Phys. Rev. Lett.* 103:248102.

22. Bai F, Lo C-J, Berry RM, & Xing J (2009) Model studies of the dynamics of bacterial flagellar motors. *Biophys. J.* 96:3154-3167.

23. Meister M, Caplan SR, & Berg HC (1989) Dynamics of a tightly coupled mechanism for flagellar rotation. *Biophys. J.* 55:905-914.

24. Brown PN, Hill CP, & Blair DF (2002) Crystal structure of the middle and C-terminal domains of the flagellar rotor protein FliG. *EMBO J.* 21:3225-3234.

25. Turner L, Ryu W, & Berg HC (2000) Real-time imaging of fluorescent flagellar filaments. *J. Bacteriol.* 182:2793-2801.

26. Sourjik V & Berg HC (2004) Functional interactions between receptors in bacterial chemotaxis. *Nature* 428:437-441.

27. Scharf BE, Fahrner KA, Turner L, & Berg HC (1998) Control of direction of flagellar rotation in bacterial chemotaxis. *Proc. Natl. Acad. Sci. USA* 95:201-206.

28. Ryu WS, Berry RM, & Berg HC (2000) Torque-generating units of the flagellar motor of *Escherichia coli* have a high duty ratio. *Nature* 403:444-447.

29. Yuan J & Berg HC (2009) Following the behavior of the flagellar rotary motor near zero load. *Exp. Mech.*

Figure Legends

Fig. 1. Normalized torque versus speed for CCW mutants (red triangles with error bars) and CW mutants (green squares with error bars). The symbols and error bars are means and standard deviations for the cell population for either mutant at each load. The red and green lines are linear regressions; see text. The load conditions were 0.356-μm-diameter latex spheres on filament stubs in 15, 12, 9, 7, 5, 3, 2 and 0% Ficoll in motility medium, and 60-nm-diameter gold spheres on hooks in motility medium (reading from left to right). The numbers of cells studied for CCW rotation at each point were 16, 18, 17, 15, 16, 15, 15, 30 and 23, respectively; the corresponding numbers for CW rotation were 15, 16, 15, 15, 15, 15, 15, 30 and 23, respectively.

Fig. 2. A. CW vs. CCW speeds. Blue filled circles with error bars (means and standard deviations for the cell population under a specific load) were obtained from measurements of wild-type cells (10-11). Reading from left to right, the loads were 2.60, 1.44, 1.20, 1.02, 0.75 and 0.356-μm-diameter latex spheres on filament stubs in motility medium, 200-nm-diameter gold spheres on hooks in 15, 10, 5 and 0% Ficoll, 150-nm-diameter gold spheres on hooks in 5 and 0% Ficoll, and 100-nm-diameter gold spheres on hooks in motility medium. The open green square with error bars is for 0.356-μm-diameter latex beads on filament stubs with the maximum possible corrections for direction-dependent variations in load included. The red open circles are measurements from switching full-length fluorescent filaments. The magenta curve was calculated from the torque-speed curves of Fig. 1, as described in **B**. The dashed line shows the curve that would be obtained were the CW and CCW speeds equivalent. **B.** CW and CCW

speeds can be extracted from the torque-speed curves (red and green lines) via their intersections with lines representing different loads; e.g., the dashed line. The torque-speed curves of Fig.1 were scaled by a factor of 350/285 to correct for difference in zero-torque speeds for strains derived from RP437 and AW405.

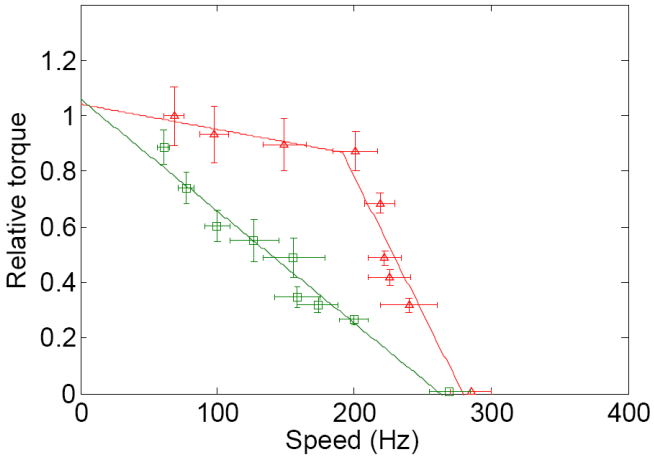

Fig. 1

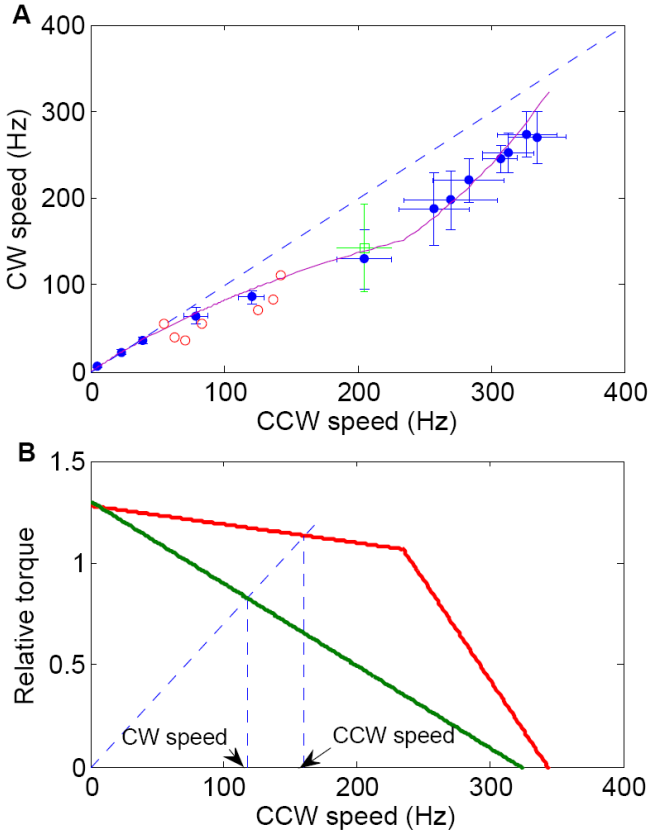
A
400
300
200
100
0
CW speed (Hz)
0
100
200
300
400
CCW speed (Hz)
B
1.5
1
0.5
0
Relative torque
CW speed
CCW speed
0
100
200
300
400
CCW speed (Hz)

Fig. 2

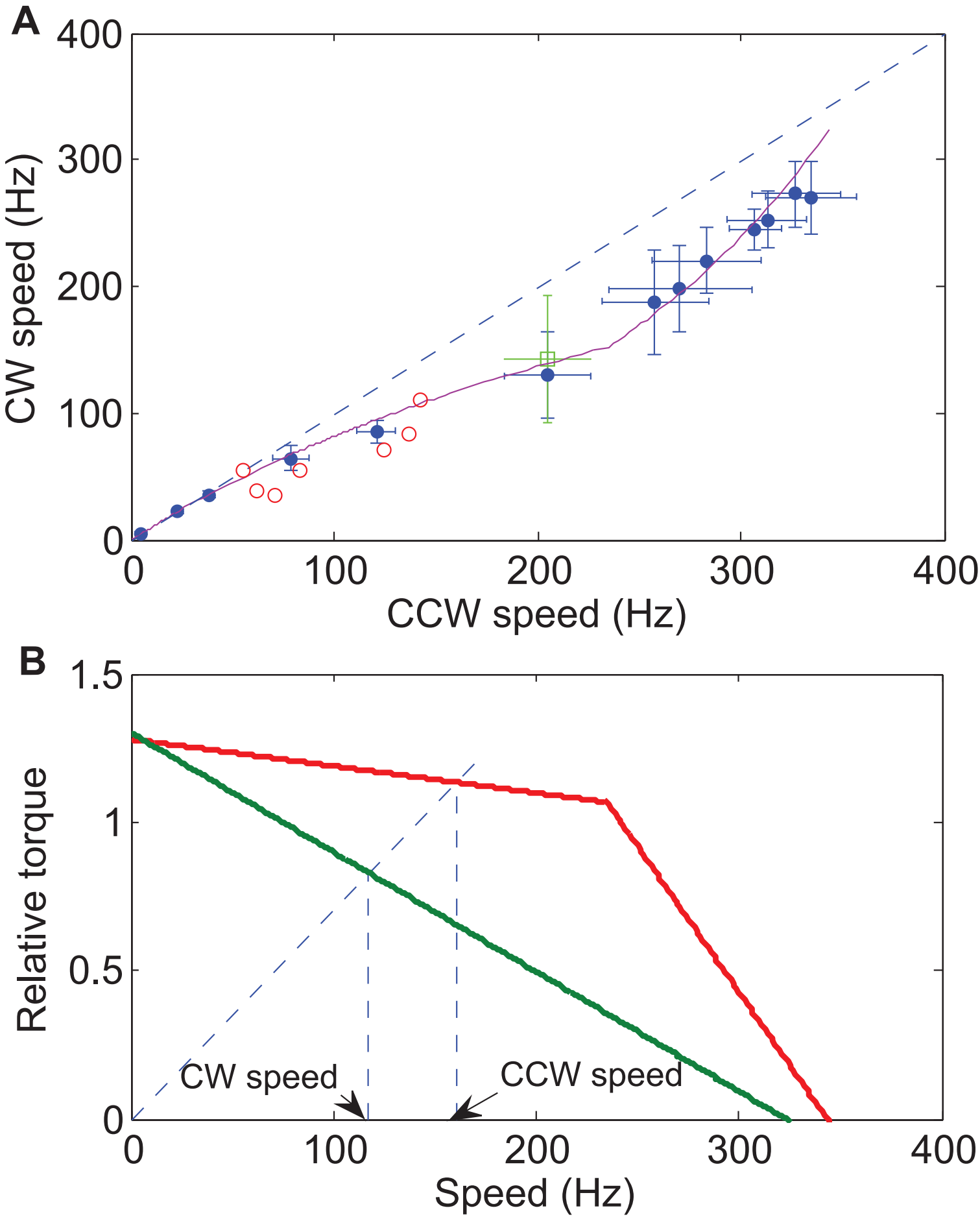
A
400
300
200
100
0
CW speed (Hz)
0
100
200
300
400
CCW speed (Hz)
B
1.5
1
0.5
0
Relative torque
CW speed
CCW speed
0
100
200
300
400
Speed (Hz)